AMG preconditioning for nonlinear degenerate parabolic equations on nonuniform grids with application to monument degradation

AMG preconditioning for nonlinear degenerate parabolic equations on nonuniform grids with application to monument degradation
APPLIED NUMERICAL MATHEMATICS, volume 68 (2012)
http://dx.doi.org/10.1016/j.apnum.2013.02.001

AMG preconditioning for nonlinear degenerate parabolic equations on nonuniform grids with application to monument degradation

M. Donatelli, M. Semplice*, S. Serra-Capizzano

Physics and Mathematics Department – University of Insubria
Via Valleggio, 11 – Como (Italy)

Abstract

Motivated by the modelling of marble degradation by chemical pollutants, we consider the approximation by implicit finite differences schemes of nonlinear degenerate parabolic equations in which sharp boundary layers naturally occur. The latter suggests to consider various types of nonuniform griddings, when defining suitable approximation schemes. The resulting large nonlinear systems are treated by Newton methods, while the locally Toeplitz linear systems arising from the Jacobian have to be solved efficiently. To this end, we propose the use of AMG preconditioners and we study the related convergence issues, together with the associated spectral features. We present some numerical experiments supporting our theoretical results on the spectrum of the coefficient matrix of the linear systems, alongside others regarding the numerical simulations in the case of the specific model.

Keywords: Nonlinear and degenerate parabolic equations, Finite differences, Newton-Krylov, Multigrid preconditioning, Flow in porous media, Marble sulfation
2010 MSC: 65M06, 65F08, 76S05

1. Introduction

The aim of this paper is to extend previous results by the authors on nonlinear implicit approximations of degenerate parabolic equations presented in [5]. In this paper we focus on nonuniform cartesian grids and on applications to the mathematical model for monument degradation described in [1] and previously approximated on uniform grids by one of the authors in [13].

We first consider a single equation of the form

$$\frac{\partial u}{\partial t} = \nabla \cdot (D(u)\nabla u)\,, \tag{1.1}$$

in both one and two-dimensional domains. We suppose that $D(u)$ is a non-negative function and note that the equation is degenerate whenever $D(u)$ vanishes. For the convergence analysis of our

*Corresponding author
Email addresses: marco.donatelli@uninsubria.it (M. Donatelli), matteo.semplice@uninsubria.it (M. Semplice), s.serrac@uninsubria.it (S. Serra-Capizzano)

numerical methods, we will require that $D(u)$ is at least differentiable and $D'(u)$ is Lipschitz continuous, while the existence of solutions is guaranteed under the milder assumption of continuity (see [19]). For the eigenvalues clustering results we require that $D(u)$ is also a nondecreasing function.

We consider a time discretization based on the so-called θ-method:

$$U(t^n, x) - \theta \Delta t L_D(U(t^n, x)) = U(t^{n-1}, x) + (1-\theta)\Delta t L_D(U(t^{n-1}, x)), \tag{1.2}$$

where $\Delta t = t^n - t^{n-1}$, and $-L_D(\cdot)$ denotes the elliptic operator $u \mapsto -\nabla \cdot (D(u)\nabla u)$. More precisely we will employ the Crank-Nicholson method ($\theta = \frac{1}{2}$) and the Implicit Euler method ($\theta = 1$). However, the analysis for a general $\theta \in (0, 1]$ is beneficial in view of the employment of the L_0-stable high order methods of [4].

The computation of the numerical solution $U(t^n, x)$ with (1.2) involves, at each timestep, the solution of a nonlinear equation whose form is determined by the operator L_D and thus by the nonlinear function $D(u)$. This, in turn, requires the use of a fixed point scheme and the choice of the Newton-like methods implies the solution, at every step of the nonlinear solver, of a large linear system whose coefficient matrix is *locally (multilevel) Toeplitz* in the sense of [17]. This matrix will be studied by its *symbol*, which describes (asymptotically) its spectrum (see [17]) and provides a useful guide for designing efficient preconditioners for linear Krylov solvers.

In [5], the case $\theta = 1$ was considered, alongside finite differences discretization on uniform grids. The nonlinear step was dealt with the Newton method, which was proved to be convergent if the time discretization step is proportional to the space discretization step. The Jacobian linear system was solved by a Krylov method preconditioned with geometric multigrid, that was proved to be optimal (in the sense that the preconditioned matrix has a strong eigenvalues cluster). Here, we extend the previous analysis to the θ-method (1.2) and to nonuniform spatial grids under the assumption that the grid points can be seen as the image of a uniform grid via an invertible function.

In order to fix ideas, consider a one-dimensional domain $\Omega = [a, b]$. Mesh points are chosen as $x_k = a + (b-a)g(k/N)$ where N and $g : [0, 1] \to [0, 1]$ control (independently) the number of mesh points and, respectively, their distribution in the domain. For problems with a still boundary or internal layer in a position known a-priori, one may get optimal meshes (in the sense of error reduction) by choosing a suitable positive *monitoring function* M and *equidistributing* it in the domain by selecting a mesh function g that satisfies (at least approximately) the relation

$$\int_0^{g(\xi)} M(s)\mathrm{d}s = \xi \int_0^1 M(s)\mathrm{d}s.$$

A typical example is that of a differential problem whose exact solution, due to a singular perturbation with parameter $\varepsilon \to 0$, presents an exponential boundary layer close to left end of the domain where $u(x) \sim e^{-x/\varepsilon}$: one can then consider a monitoring function of the form

$$M(s) = \max\left\{1, \tfrac{1}{\varepsilon} e^{-s/\varepsilon}\right\}$$

and obtain a Bakhvalov-type mesh on which the convergence properties of the numerical approximation are uniform in the perturbation parameter. For a general introduction, examples and other types of meshes, see e.g. [11] and references therein.

However, the PDE system introduced in [1] for marble sulfation has solutions that feature a sharp internal layer that forms at the interface between the marble and the polluted air (boundary

of the computational domain) and that moves towards the inside of the monument as degradation progresses. This layer separates the outer gypsum crust from the inner pristine marble.

Hence optimal choices for a mesh to be kept fixed in time are not available for this problem, but we are still interested in non-uniform meshes for the two following reasons. First, from a theoretical point of view, in this paper we do not focus on the appropriateness of the choice of the mesh in the sense of error reduction, but rather on the analysis of the nonlinear and linear systems arising from a given choice of mesh and on developing a robust preconditioning strategy in the case of nonuniform meshes. To this end, the choice of the mesh function g in some numerical tests will not be guided by error reduction, but by the need to test the theoretical results on a wide range of cases. Secondly, from a modelling point of view, restoration works must take place on a monument before the internal layer has moved too deeply into the domain and thus practical computations can be performed on a fixed nonuniform grid that is finer close to the boundary where the internal layer will form.

Finally, we point out that, obviously, the discretization and resolution technique studied here can be plugged into a more general method that employs finite element discretizations and/or adaptive mesh refinement. Regarding the discretization with finite elements, there exists a kind of information depending only on the continuous operator and which is inherited virtually unchanged in both finite differences and finite elements, provided that the grids are quasi-uniform in finite differences and the angles are not degenerating in finite elements. Such information consists in the locally Toeplitz structure used and in the related spectral features: conditioning, subspaces related to small eigenvalues, global spectral behaviour, etc. (see [17] and [2]).

The paper is organized as follows. In Section 2 we describe the space discretization of (1.1) by nonuniform finite difference grids. For the time discretization we use the θ-method (1.2) which leads to a system of coupled nonlinear equations that need to be solved at each discrete timestep: this is achieved using the Newton method, as detailed in Section 3. In Section 4 we propose an algebraic multigrid preconditioner for the Jacobian matrix appearing in the Newton method and provide an analysis of the spectrum of the preconditioned matrix that proves the effectiveness of our proposal. In Section 5 we discretize a model for the chemical aggression on marble stones that consists in a system of two partial differential equations and extend the previous results to this setting. Finally, in Section 6, we perform some numerical tests.

2. Finite difference space discretization of the operator $L_D(\cdot)$

2.1. One space dimension

Let $g : [0, 1] \to [a, b]$ a nondecreasing differentiable function such that $g(0) = a$ and $g(1) = b$. Consider the grid composed by the points $x_k = g(k/(N + 1))$, for $k = 0, \ldots, N + 1$. We denote by u_k^n the approximate solution at time t^n and location x_k, where $k = 0, \ldots, N+1$. When considering Dirichlet boundary conditions, the values u_0 and u_{N+1} are known and can be eliminated by the equations. Let thus $\mathbf{u}^n$ be the vector of size N containing the collection of the values u_k^n. for $k = 1, \ldots, N$. When no potential confusion arises, we sometimes drop in both notations the superscript indicating the time level. Boundary conditions of Neumann or Robin type can be treated in similar ways.

We denote by $\mathsf{tridiag}_k^N[\beta_k, \alpha_k, \gamma_k]$ a square tridiagonal matrix of order N where the k^{th} row has entries β_k on the lower diagonal, α_k on the main diagonal, and γ_k on the upper diagonal. We also denote with $\mathsf{diag}_k^N(\alpha_k)$ the square $N \times N$ diagonal matrix with α_k on the k^{th} row.

We choose a standard 3-points second order approximation of the differential operator $(D(u)u_x)_x$. Let $x_{j+1/2} = (x_j + x_{j+1})/2$ and $h_j = x_j - x_{j-1}$. Denoting by the subscript ξ the numerical approximation of a quantity at the point x_ξ, we have

$$\frac{\partial}{\partial x}\left(D(u)\frac{\partial u}{\partial x}\right)\bigg|_{x_j} = \frac{D_{j+1/2}\frac{u_{j+1}-u_j}{h_{j+1}} - D_{j-1/2}\frac{u_j-u_{j-1}}{h_j}}{(h_j + h_{j+1})/2} + o(1), \tag{2.1}$$

where we define

$$D_{j+1/2} = \frac{D(u_{j+1}) + D(u_j)}{2}, \qquad j = 0, \ldots, N,$$

and the $o(1)$ error term is of order h^2 under the assumption that the composition $D(u(\cdot))$ is at least continuously differentiable, with Lipschitz continuous first derivative. Note that, at least for $D(u) = u^m$, a solution u is at least Hölder continuous [19, Chap. 2]. Moreover, defining the *positivity set* $\mathcal{P}(t) = \{x \in \Omega : u(t, x) > 0\}$, one shows that for reasonable initial data, $\mathcal{P}(t)$ is expanding with finite speed and that the solution u is regular in the interior of $\mathcal{P}(t)$ and has a singularity on its boundary [19, Chap. 14]. Thus the precision of the finite difference formula is degraded only on $\partial\mathcal{P}(t)$, a set of measure zero in Ω, but of course the method is expected to be of first order accuracy in the case of a degenerate parabolic equation, as shown in the numerical tests.

Putting together all the contributions for different grid points, the action of the elliptic differential operator on $\mathbf{u}$ is described by the tridiagonal matrix

$$-L^{(1)}_{D(\mathbf{u})} = \mathrm{diag}^N_k\left[\frac{2}{h_k + h_{k+1}}\right]\mathrm{tridiag}^N_k\left[-\frac{D_{k-1/2}}{h_k}, \frac{D_{k-1/2}}{h_k} + \frac{D_{k+1/2}}{h_{k+1}}, -\frac{D_{k+1/2}}{h_{k+1}}\right]. \tag{2.2}$$

Remark 2.1. $L^{(1)}_{D(\mathbf{u})}$ is similar to a symmetric real tridiagonal matrix. If $D(u(\cdot))$ is a nonnegative function, then the matrix $-L^{(1)}_{D(\mathbf{u})}$ has always nonnegative eigenvalues, since it is weakly diagonally dominant by row. Furthermore, in the previous sentence the word *nonnegative* can be replaced by *positive* if the equation is not degenerate.

2.2. Two space dimensions

The discretization considered above can be extended to the two-dimensional case as follows. We consider the domain $\Omega = [a_1, b_1] \times [a_2, b_2] \subset \mathbb{R}^2$ and the grid points $x_{i,j} = (g^{[1]}(i/(N + 1)), g^{[2]}(j/(N + 1)))$, where $g^{[i]} : [0, 1] \to [a_i, b_i]$, $i = 1, 2$ are nondecreasing differentiable functions. The grid is thus composed of the $(N + 2)^2$ points $x_{i,j}$ for i and j ranging from 0 to $N + 1$. We denote with $u_{i,j}$ the numerical value approximating $u(x_{i,j})$. Of course, as in the one-dimensional case the use of Dirichlet boundary conditions reduces the gridding to the N^2 internal points; also in this case other boundary conditions can be considered in a similar way. With this choice, the grid spacing is $h^{[1]}_k = x_k - x_{k-1}$ and $h^{[2]}_k = y_k - y_{k-1}$.

The finite difference discretization of the differential operator (2.1) can be generalised as follows:

$$\begin{aligned}\frac{\partial}{\partial x}\left(D(u)\frac{\partial u}{\partial x}\right)\bigg|_{x=x_{i,j}} &+ \frac{\partial}{\partial y}\left(D(u)\frac{\partial u}{\partial y}\right)\bigg|_{x=x_{i,j}} \\ &= \frac{D_{i+1/2,j}\frac{u_{i+1,j}-u_{i,j}}{h^{[1]}_{i+1}} - D_{i-1/2,j}\frac{u_{i,j}-u_{i-1,j}}{h^{[1]}_i}}{(h^{[1]}_i + h^{[1]}_{i+1})/2} + \frac{D_{i,j+1/2}\frac{u_{i,j+1}-u_{i,j}}{h^{[2]}_{j+1}} - D_{i,j-1/2}\frac{u_{i,j}-u_{i,j-1}}{h^{[2]}_j}}{(h^{[2]}_j + h^{[2]}_{j+1})/2} + o(1)\end{aligned} \tag{2.3}$$

where we denoted

$$D_{i+1/2,j} = \frac{D(u_{i+1,j}) + D(u_{i,j})}{2} \qquad \text{and} \qquad D_{i,j+1/2} = \frac{D(u_{i,j+1}) + D(u_{i,j})}{2},$$

and where the term $o(1)$ is $O(h^2)$ if $D(u(\cdot))$ is smooth enough.

Collecting the unknowns $u_{i,j}$ in a vector $\mathbf{u}$ using the lexicographical ordering, we denote by $L^{(2)}_{D(\mathbf{u})}$ the matrix representing the differential operator. This matrix has the same sparsity pattern as the tensor product $L^{(1)}_D \otimes I_N + I_N \otimes L^{(1)}_D$, but the entries are different. More precisely, $L^{(2)}_{D(\mathbf{u})} = A + B$ where A is block-diagonal with 3-diagonal blocks and B is block 3-diagonal with diagonal blocks. In particular, the generic (j, j) block of A is the matrix $L^{(1)}_{D(u_{\cdot,j})}$, which is given by formula (2.2) applied with the $D(u)$ evaluated on the unknowns $u_{\cdot,j}$ on the horizontal segment $y = y_j$. Similarly the j-th block row of B corresponds to the matrix $L^{(1)}_{D(u_{j,\cdot})}$. When needed, appropriate finite rank corrections for boundary conditions are also included in the first/last blocks of A and first/last rows of the blocks in B. Notice that the pattern of the matrix $L^{(2)}_{D(\mathbf{u})}$ reminds a tensor structure that unfortunately cannot be formalised exactly if the function $D(u)$ is not separable, due to the varying coefficients in the underlying PDE (for the spectral analysis of such structures refer to [14] and references therein).

3. Time discretization and the Newton's method

Following (1.2), at each timestep, we need to solve the nonlinear vector equation

$$\mathbf{u}^n = \mathbf{u}^{n-1} + \theta\Delta t L^{(d)}_{D(\mathbf{u}^n)}\mathbf{u}^n + (1-\theta)\Delta t L^{(d)}_{D(\mathbf{u}^{n-1})}\mathbf{u}^{n-1} \tag{3.1}$$

where $d = 1, 2$ is the number of space dimensions. Thus we set up Newton iterations for the vector function

$$F(\mathbf{u}) = \mathbf{u} - \theta\Delta t L^{(d)}_{D(\mathbf{u})}\mathbf{u} - (1-\theta)\Delta t L^{(d)}_{D(\mathbf{u}^{n-1})}\mathbf{u}^{n-1} - \mathbf{u}^{n-1}. \tag{3.2}$$

The Jacobian of $F(\mathbf{u})$ can be written as

$$F'(\mathbf{u}) = X^{(d)}_N(\mathbf{u}) + Y^{(d)}_N(\mathbf{u}), \tag{3.3a}$$

where, denoting by I_{N^d} the identity matrix of order N^d, we have

$$X^{(d)}_N(\mathbf{u}) = I_{N^d} - \theta\Delta t L^{(d)}_{D(\mathbf{u})} \tag{3.3b}$$

and $Y^{(d)}_N(\mathbf{u})$ contains the terms arising from differentiating the matrix $L^{(d)}_{D(\mathbf{u})}$ with respect to $\mathbf{u}$ and is defined below. We note that according to Remark 2.1, the matrix $X^{(1)}_N(\mathbf{u})$ is similar to a symmetric positive definite matrix having minimum eigenvalue $\lambda_{\min}(X^{(1)}_N(\mathbf{u})) \geq 1$.

In the one-dimensional case

$$Y^{(1)}_N(\mathbf{u}) = \theta\Delta t\, \mathrm{diag}^N_k\left[\tfrac{1}{h_k+h_{k+1}}\right] T^{(1)}_N(\mathbf{u})\mathrm{diag}^N_k[D'_k] \tag{3.3c}$$

$$T^{(1)}_N(\mathbf{u}) = \mathrm{tridiag}^N_k\left[-\tfrac{u_k-u_{k-1}}{h_k},\ \tfrac{u_{k+1}-u_k}{h_{k+1}} - \tfrac{u_k-u_{k-1}}{h_k},\ \tfrac{u_{k+1}-u_k}{h_{k+1}}\right]. \tag{3.3d}$$

Here D'_k denotes $D'(u_k)$. In the two-dimensional case, $Y^{(2)}_N(\mathbf{u})$ is obtained from the one-dimensional analogues in the same way as $L^{(2)}_D$ is obtained from the $L^{(1)}_D$'s. In particular it has the same nonzero pattern of $Y^{(1)}_N \otimes I_N + I_N \otimes Y^{(1)}_N$.

In the case of a uniform spatial grid with discretization step equal to h, in [5] the convergence of Newton's method was proved assuming that the initial guess is the solution at the previous time step and $\Delta t \leq Ch$, for a positive constant C independent of h. Accordingly, we fix

$$\Delta t = h = \frac{1}{N+1}. \tag{3.4}$$

The numerical experiments in Section 6 show that the Newton's method usually converges fast enough with such choice of Δt. Note that this is appropriate for the theoretical analysis in the following section, since the domain of g is $[0, 1]$ and that one would consider the real domain size in a practical situation.

At each Newton iteration, we need to solve a linear system whose coefficient matrix is represented by the Jacobian $F'(\mathbf{u})$. In principle, the Jacobian is recomputed at each Newton iteration, so we are interested in efficient iterative methods for the linear system. To this end, we first analyse the spectral properties of the matrix $F'(\mathbf{u})$. This will lead us to consider preconditioned Krylov methods, with an algebraic multigrid preconditioner [12].

4. Asymptotic spectral analysis of the preconditioned Jacobian sequence

Since we are interested in nonuniform grids, we follow the analysis of [15]. The difficulty arising from the non-uniformity can be overcome by reinterpreting the nonuniform grid Jacobian matrices as an approximation of uniform grid Jacobian matrices coming from a different continuous problem which still has the form (1.1), but a new weight function and a different domain. In this way we can successfully apply the preconditioning technique just proposed in the case of an equispaced grid-sequence [5].

4.1. Preliminary definitions

The following classification of sequence of grids $\mathcal{G} = \{\mathcal{G}_N\}$ will be useful to analyse the spectral distribution and the preconditioning strategy of the Jacobian matrix sequence.

Definition 4.1 ([15])**.** A grid sequence $\mathcal{G} = \{\mathcal{G}_N\}$ on $[a, b]$, $\mathcal{G}_N = \{x_0 = a < x_1 < \cdots < x_N < x_{N+1} = b\}$, is said to be *weakly equivalent* to the grid sequence $\mathcal{W} = \{\mathcal{W}_N\}$ on $[c, d]$, $\mathcal{W} = \{y_0 = c < y_1 < \cdots < y_N < y_{N+1} = d\}$, if there exists a function g so that $g(y_j) = x_j$. The function g is required to be a homeomorphism from $[a, b]$ to $[c, d]$, to be piecewise C^1 with g' having at most a finite number of discontinuity points and a finite number of zeros. Moreover, if both g and its inverse g^{-1} are Lipschitz continuous, then $\mathcal{G}$ is said to be equivalent to $\mathcal{W}$.

Definition 4.2 ([15])**.** A grid sequence $\mathcal{G}$ is said to be *(weakly) regular* if it is (weakly) equivalent to the basic equispaced grid sequence $\mathcal{U} = \{\mathcal{U}_N\}$ on $[0, 1]$, with $g : [0, 1] \to [a, b]$ being the associated homeomorphism according to Definition 4.1.

For example, the grid sequence associated to the Gauss-Lobatto points is weakly regular: in fact, they correspond to the choice $g(x) = \cos(\pi x)$, whose derivative $g'(x)$ is smooth and with a unique zero in $[0, 1]$. The Bakhvalov grid generated by the monitoring function mentioned in the Introduction is regular for any finite ε, since $g'(0) \sim \varepsilon$ (see (5.2)).

In order to design fast iterative solvers, we analyse the asymptotical behaviour of the spectrum of the Jacobian matrix when N goes to infinity. In the following, we study asymptotical quantities associated to matrix sequences whose definition is reported below.

Definition 4.3. Let $\{A_N\}_{N\in\mathbb{V}}$ denote a sequence of matrices where the set of nonnegative indices $\mathbb{V}$ is of infinite cardinality and where the matrix A_N is a square matrix of order N with complex entries.

A sequence of matrices $\{A_N\}$ naturally arises considering the same discretization of the same differential or integral equation for a sequence of grids with an increasing number of points or elements.

Definition 4.4. Let $C_0(\mathbb{C})$ be the set of continuous functions with bounded support defined over the complex field, d be a positive integer, and ψ be a complex-valued measurable function defined on a set $G \subset \mathbb{R}^d$ of finite and positive Lebesgue measure $\mu(G)$. A matrix sequence $\{A_N\}$ is said to be *distributed* (*in the sense of the eigenvalues*) *as the pair* (ψ, G), or to *have the eigenvalue distribution function* ψ ($\{A_N\} \sim_\lambda (\psi, G)$), if, $\forall F \in C_0(\mathbb{C})$, the following limit relation holds

$$\lim_{N\to\infty} \frac{1}{N} \sum_{j=1}^{N} F\left(\lambda_j(A_N)\right) = \frac{1}{\mu(G)} \int_G F(\psi)\, d\mu, \qquad t = (t_1, \ldots, t_d), \tag{4.1}$$

where $\lambda_j(A_N)$ ranges over the spectrum of A_N for $j = 1, \ldots, N$.

Example 4.5. *The matrix* $A_N = \mathsf{tridiag}_k^N[-1,\ 2\ -1]$ *is related to the second order finite difference discretization of the second derivative in one spatial dimension. It is well-known that* $\lambda_j(A_N) = 2 - 2\cos\left(\frac{j\pi}{n+1}\right)$, *for* $j = 1, \ldots, n$. *Hence* $\{A_N\} \sim_\lambda (2 - 2\cos(x), (0, \pi))$ *according to Definition 4.4.*

Along with the distribution in the sense of eigenvalues, for the practical convergence analysis of iterative solvers we are also interested in a further asymptotic property called *clustering*.

Definition 4.6. A matrix sequence $\{A_N\}$ is *clustered at* $S \subset \mathbb{C}$ (in the eigenvalue sense), if for any $\varepsilon > 0$ the number of the eigenvalues of A_N outside the disks

$$D(S, \varepsilon) = \bigcup_{s\in S} D(s, \varepsilon), \qquad D(s, \varepsilon) := \{z : |z - s| < \varepsilon\}$$

is $o(N)$. In other words

$$q_\varepsilon(N, s) := \#\{\lambda_j(A_N) : \lambda_j \notin D(S, \varepsilon)\} = o(N), \quad N \to \infty.$$

If every A_N has only real eigenvalues (at least for all N large enough), then any $s \in S$ is real and the related disk $D(s, \varepsilon)$ reduces to the interval $(s - \varepsilon, s + \varepsilon)$. The cluster is strong if the term $o(N)$ is replaced by $O(1)$ so that the number of outlying eigenvalues is bounded by a constant not depending on the size N of the matrix.

We say that a preconditioner P_N is optimal for A_N if the sequence $\{P_N^{-1}A_N\}$ is clustered at one (or to any constant with positive real part) in the strong sense. Of course, the optimality is also reached if the clustering is at a set S, with S contained in a complex box $[\alpha, \beta] \times \mathrm{i}[-\gamma, \gamma]$ with α, β, γ independent of N and $0 < \alpha \le \beta$: as already mentioned a very interesting case occurs when S contains just a point or a finite number of points.

The (weak or general) clustering is also of interest as a heuristic indication that the preconditioner is effective.

Remark 4.7. $\{A_N\} \sim_\lambda (\psi, G)$ with $\psi \equiv s$ a constant function is equivalent to $\{A_N\}$ being clustered at $s \in \mathbb{C}$.

The previous Definitions 4.4 and 4.6 can be stated also for the singular values just replacing λ with σ and *eigenvalue* with *singular value*.

Definition 4.8. A sequence of matrices $\{A_N\}$ is *sparsely vanishing* if and only if $\forall M > 0$, $\exists N_M$ s.t. $\forall N \geq N_M$ it holds

$$\#\{i : \sigma_i(A_N) < 1/M\} \leq r(M)N, \qquad \lim_{M\to\infty} r(M) = 0.$$

Remark 4.9. If $\{A_N\} \sim_\sigma \phi$ with measurable ϕ, then $\{A_N\}$ is sparsely vanishing if and only if ϕ is sparsely vanishing, that is $\lim_{M\to\infty} \mu\{x : |\phi(x)| < 1/M\} = 0$ with $\mu\{\cdot\}$ denoting the usual Lebesgue measure.

Remark 4.10. The notion of sparsely vanishing matrix sequence is important in the context of preconditioning. Let us assume that $\{P_N\}$ is used as a preconditioning matrix sequence for $\{A_N\}$: if $\{A_N - P_N\}$ is clustered at zero, then $\{P_N^{-1}A_N\}$ is clustered at 1 if in addition $\{P_N\}$ (and a fortiori $\{A_N\}$) is sparsely vanishing. The latter argument is crucial in the proof of Theorem 4.14.

For a matrix A, we will denote by $\|A\|$ the spectral norm, i.e. the largest singular value, and by $\|A\|_{\text{tr}}$ the trace norm, that is the sum of all singular values. For the following results, we freely exploit the algebra structure of the locally Toeplitz matrices introduced in [17] and its extension, the algebra of Generalized Locally Toeplitz (GLT) in [14]. For the spectral distribution of non-symmetric matrix sequences, the results in [6] are of crucial importance. In particular, we report the following theorem, where a basic test on the trace norm of a perturbation C_N allows to conclude that $\{A_N = B_N + C_N\}$ has the same eigenvalue distribution as $\{B_N\}$, provided that, for every N, B_N is Hermitian.

Theorem 4.11 ([6])**.** *Let $\{B_N\}$ and $\{C_N\}$ be two matrix sequences, where B_N is Hermitian and $A_N = B_N + C_N$. Assume further that $\{B_N\} \sim_\lambda (\psi, G)$, G of finite and positive Lebesgue measure, both $\|B_N\|$ and $\|C_N\|$ are uniformly bounded by a constant independent of N, and $\|C_N\|_{\text{tr}} = o(N)$, $N \to \infty$. Then ψ is real valued and $\{A_N\} \sim_\lambda (\psi, G)$.*

4.2. Algebraic multigrid preconditioning

The Jacobian $F'(\mathbf{u})$ is not symmetric, so we suggest to solve the linear system by preconditioned GMRES (PGMRES), in particular using the algebraic multigrid in [12] as preconditioner. We point out that, with this choice, the method converges in few iterations and we have to memorise only few vectors, without resorting to a restart procedure.

Firstly, we prove that the matrix $X_N^{(d)}(\mathbf{u})$, $d = 1, 2$, is a M-matrix and it is an effective preconditioner for $F'(\mathbf{u})$. Finally, since, as already observed in Section 3, $X_N^{(d)}(\mathbf{u})$, $d = 1, 2$, is similar to a symmetric positive definite matrix and since the AMG is an optimal solver for symmetric M-matrices [12], we conclude that it is an effective preconditioner for $F'(\mathbf{u})$.

There are several equivalents definitions of M-matrix (see [9]). We use the following.

Definition 4.12. A square matrix is a *M-matrix* if it has all off-diagonal entries less than or equal to zero and all eigenvalues have positive real part.

Proposition 4.13. *The matrix $X_N^{(d)}(\mathbf{u})$, $d = 1, 2$, defined in* (3.3b) *is a M-matrix.*

Proof. Since $D(u)$ is a nonnegative function, (3.3b) shows that all off-diagonal entries of $X_N^{(d)}(\mathbf{u})$ are less than or equal to zero. Moreover, the diagonal entries of $X_N^{(d)}(\mathbf{u})$ are positive and $X_N^{(d)}(\mathbf{u})$ is diagonally dominant. Therefore, thanks to the Gershgorin's theorem (Theorem 6.9.4 in [16]), the eigenvalues are contained in the union of disks which are contained in the positive complex half plane. □

Even if the matrix $X_N^{(d)}(\mathbf{u})$, $d = 1, 2$, is not symmetric, it can be easily rescaled to be symmetric. Hence, by Proposition 4.13 and the optimality of AMG for symmetric M-matrices, we obtain that the AMG converges in a constant number of iterations when applied to linear systems with coefficient matrix $X_N^{(d)}(\mathbf{u})$, $d = 1, 2$.

Now we prove that $X_N^{(d)}(\mathbf{u})$ is an effective preconditioner for $F'(\mathbf{u})$, describing in detail the spectral analysis for the one-dimensional case and just sketching its extension to the two-dimensional case. The following theorem shows that both the eigenvalues and the singular values of the preconditioned matrices sequence cluster at 1.

Theorem 4.14. *Consider a (weakly) regular sequence of grids according to Definition 4.1, $G = [0, 1] \times (0, 2\pi)$ and assume that $D \neq 0$ a.e.. If $\frac{\mathrm{d}}{\mathrm{d}u} D(u) \geq 0$ then*

$$\{(X_N^{(1)}(\mathbf{u}))^{-1} F'(\mathbf{u})\} \sim_\lambda (1,\, G).$$

Otherwise

$$\{(X_N^{(1)}(\mathbf{u}))^{-1} F'(\mathbf{u})\} \sim_\sigma (1,\, G).$$

Proof. Define the diagonal positive definite matrix

$$S_N = \mathrm{diag}_k^N \left[\frac{2}{h_k + h_{k+1}} \right]. \tag{4.2}$$

that provides a diagonal scaling useful to prove the clustering result. From equation (3.3),

$$(X_N^{(1)}(\mathbf{u}))^{-1} F'(\mathbf{u}) = I_N + (X_N^{(1)}(\mathbf{u}))^{-1} Y_N^{(1)}(\mathbf{u}) = I_N + (S_N^{-1} X_N^{(1)}(\mathbf{u}))^{-1} S_N^{-1} Y_N^{(1)}(\mathbf{u}),$$

and thus the sequence $\{(X_N^{(1)}(\mathbf{u}))^{-1} F'(\mathbf{u})\}$ is clustered at one if the sequence $\{S_N^{-1} Y_N^{(1)}(\mathbf{u})\}$ is clustered at zero and $\{S_N^{-1} X_N^{(1)}(\mathbf{u})\}$ is sparsely vanishing (see [15, Theor. 3.6]). Indeed, the clustering at zero of $\{S_N^{-1} Y_N^{(1)}(\mathbf{u})\}$ is not enough to ensure the clustering at zero of the sequence $\{B_N\}$ of the whole matrix $B_N = (S_N^{-1} X_N^{(1)}(\mathbf{u}))^{-1} S_N^{-1} Y_N^{(1)}(\mathbf{u})$, because, roughly speaking, if $\{S_N^{-1} X_N^{(1)}(\mathbf{u})\}$ is not sparsely vanishing it amplifies the eigenvalues of the matrix B_N (see Remark 4.10).

First, we prove that $\{S_N^{-1} X_N^{(1)}(\mathbf{u})\}$ is sparsely vanishing. From equation (3.3b), it holds

$$S_N^{-1} X_N^{(1)}(\mathbf{u}) = S_N^{-1} - \theta h S_N^{-1} L_{D(\mathbf{u})}^{(1)}. \tag{4.3}$$

The grid points are defined as $x_k = g(z_k)$ where $z_k = k/(N + 1)$, $k = 0, \ldots, N$. Therefore $z_{k+1} - z_k = h$ and

$$h_{k+1} + h_k = g(z_{k+1}) - g(z_{k-1}) = 2h g'(\xi_k), \qquad \xi_k \in (z_{k-1}, z_{k+1}).$$

It follows that

$$\{S_N^{-1}\} \sim_\lambda (0, G), \tag{4.4}$$

since $g'(x)$ is bounded. The matrix $-h S_N^{-1} L_{D(\mathbf{u})}^{(1)}$ is a positive semidefinite matrix and its spectral distribution was already studied in [15, Theor. 3.7]. In detail

$$\{-h S_N^{-1} L_{D(\mathbf{u})}^{(1)}\} \sim_\lambda (\psi_1,\, G), \tag{4.5}$$

where $G = [0,1] \times (0, 2\pi)$ and

$$\psi_1(x,s) = \tilde{w}^{[D]}(x)(2 - 2\cos(s)),$$
$$\tilde{w}^{[D]}(x) = \begin{cases} \frac{D(u(g(x)))}{g'(x)}, & \text{if } g'(x) \text{ is defined and nonzero,} \\ 1, & \text{otherwise,} \end{cases}$$

For a (weakly) regular sequence of grids the function ψ_1 is sparsely vanishing. Therefore, applying Theorem 4.11 to the splitting (4.3), thanks to (4.4) and (4.5), we have that

$$\{S_N^{-1} X_N^{(1)}(\mathbf{u})\} \sim_\lambda (\theta\psi_1, G)$$

and thus the sequence $\{S_N^{-1} X_N^{(1)}(\mathbf{u})\}$ is sparsely vanishing according to Remark 4.9.

Now we prove that $\{S_N^{-1} Y_N^{(1)}(\mathbf{u})\}$ is clustered at zero observing that

$$S_N^{-1} Y_N^{(1)}(\mathbf{u}) = \frac{\theta\Delta t}{2}\, T_N^{(1)}(\mathbf{u}) \mathsf{diag}_k^N[D'_k]. \tag{4.6}$$

In order to estimate the eigenvalue distribution of $T_N^{(1)}(\mathbf{u})$ in (3.3d), we preliminarily observe that

$$\begin{aligned} \frac{u(x_{k+1}) - u(x_k)}{h_{k+1}} &= \frac{u(g(z_{k+1})) - u(g(z_k))}{z_{k+1} - z_k} \frac{z_{k+1} - z_k}{g(z_{k+1}) - g(z_k)} \\ &= \frac{u'(g(\tilde{\xi}_k))g'(\tilde{\xi}_k)}{g'(\hat{\xi}_k)}, \end{aligned} \tag{4.7}$$

where $\tilde{\xi}_k, \hat{\xi}_k \in (z_k, z_{k+1})$. Owing to well-known results on Toeplitz matrices (see [7]), it holds that

$$\{\mathsf{tridiag}_k^N[-1,0,1]\} \sim_\lambda (\mathrm{i}2\sin(s), (0,2\pi)). \tag{4.8}$$

Since the diagonal of $T_N^{(1)}(\mathbf{u})$ represents a lower order term, due to (4.7), we have

$$T_N^{(1)}(\mathbf{u}) = \mathsf{diag}_k^N[u'(g(\tilde{\xi}_k))]\mathsf{tridiag}_k^N[-1,0,1] + E_N$$

where E_N has infinitesimal spectral norm, so that $\{E_N\} \sim_\lambda (0, G)$. Furthermore a direct computation shows that $\{\mathsf{diag}_k^N[u'(g(\tilde{\xi}_k))]\} \sim_\lambda (u'(g(x)), [0,1]))$. However, the sequences

$$\{E_N\},\ \{\mathsf{diag}_k^N[u'(g(\tilde{\xi}_k))]\},\ \{\mathsf{tridiag}_k^N[-1,0,1]\}$$

are GLT sequences with symbols $0, u'(g(x)), \mathrm{i}2\sin(s)$, and the set of all GLT sequences forms an algebra (see [14]), and in particular any linear combination of products of GLT sequences is a new GLT sequence having as symbol the same linear combination of products of the basic symbols. As a consequence, by combining equations (4.7), (4.8), the previous argument, and taking into account the antisymmetric part of $T_N^{(1)}(\mathbf{u})$ has $o(N)$ trace norm, by Theorem 4.11, we conclude that

$$\{T_N^{(1)}(\mathbf{u})\} \sim_\lambda (\mathrm{i}2u'(g(x))\sin(s), G). \tag{4.9}$$

Hence, from equation (4.6) it follows that $\{S_N^{-1} Y_N^{(1)}(\mathbf{u})\} \sim_\lambda (0, G)$.

If $D'(u) \geq 0$, by equation (4.6) and the similarity transformation

$$\mathsf{diag}_k^N[D'_k]^{1/2} S_N^{-1} Y_N^{(1)}(\mathbf{u}) \mathsf{diag}_k^N[D'_k]^{-1/2} = \frac{\theta\Delta t}{2}\, \mathsf{diag}_k^N[D'_k]^{1/2}\, T_N^{(1)}(\mathbf{u}) \mathsf{diag}_k^N[D'_k]^{1/2}, \tag{4.10}$$

we obtain an antisymmetric matrix that, up to a lower order term, shows spectral norm going to zero as h tends to zero. Therefore, thanks to Theorem 4.11, we are allowed to consider only the symmetric part and hence we obtain that $\{S_N^{-1} Y_N^{(1)}(\mathbf{u})\}$ has also an eigenvalue cluster at zero. □

Remark 4.15. The assumption $D'(u) \geq 0$ is often satisfied in the applications, e.g. in all phenomena described by the heat equation with constant diffusion coefficient and by the porous media equation, i.e. the PDE (1.1) with $D(u) = mu^{m-1}$ for $m > 1$ (see e.g. [19, Chap. 2]).

As already observed in Remark 4.15, in real applications, some assumptions concerning $D(u(x))$ have to be considered. For instance, in the one-dimensional setting, a practical situation occurs when $u(x)$, and thus $D(u)$, vanishes identically in some nontrivial sub-interval. This situation is not covered by Theorem 4.14 where we required that D is positive a.e.: however the argument that proves Theorem 4.14 can be used again under the general assumption that D vanishes on a finite number of disjoint nontrivial closed intervals and it is positive a.e. in the rest of the domain. More precisely, by looking at the expressions in (2.2), (3.3), and assuming k nontrivial disjoint closed sub-intervals $J_0, \ldots, J_k$ in which u vanishes, we observe that both $X_N^{(1)}(\mathbf{u})$ and $F'(\mathbf{u})$ essentially decompose in a direct sum with blocks of the same size with identities of appropriate size corresponding to the samplings where u is identically zero.

More in detail, let $\left(\bigcup_{i=0}^{k+1} K_i\right) \cup \left(\bigcup_{i=0}^{k} J_i\right)$ be a partition of the whole domain $[a, b]$, where K_0 and K_{k+1} may be empty. For a matrix $M_N \in \mathbb{R}^{N\times N}$ define the restriction $M_N|_{K_j}$ to be the diagonal block of M_N corresponding to the indices in K_j and the decomposition

$$\mathcal{D}(M_N) = M_N|_{K_0} \oplus I_{J_0} \oplus M_N|_{K_1} \oplus \cdots \oplus M_N|_{K_k} \oplus I_{J_k} \oplus M_N|_{K_{k+1}},$$

where for square matrices A and B, of size μ and ν, respectively, its direct sum $A \oplus B$ has size $\mu + \nu$ and is defined as the following block diagonal matrix

$$A \oplus B = \begin{bmatrix} A & 0 \\ 0 & B \end{bmatrix}.$$

By examining the entries of the Jacobian matrix (3.3) we have that

$$X_N^{(1)}(\mathbf{u}) = \mathcal{D}(X_N^{(1)}(\mathbf{u})) + \widetilde{R}_{N,k}, \qquad F'(\mathbf{u}) = \mathcal{D}(F'(\mathbf{u})) + R_{N,k},$$

where the terms $R_{N,k}$ and $\widetilde{R}_{N,k}$ have rank not exceeding $4(k + 1)$. In order to understand the latter statement, denote with l_j and L_j, $j = 0, \ldots, k + 1$, the first and the last index in K_j, and observe that the elements

$$(F'(\mathbf{u}))_{l_j, l_j-1}, \qquad (F'(\mathbf{u}))_{l_j-1, l_j}, \qquad (F'(\mathbf{u}))_{l_j-1, l_j-1}$$

are generically nonzero, while the corresponding positions of $\mathcal{D}(F'(\mathbf{u}))$ are null by construction. Moreover, the same holds replacing l_j and $l_j - 1$ in the previous formula with L_j and $L_j + 1$ respectively and both remarks are valid for $X_N(\mathbf{u})$ too. Thus $R_{N,k}$ and $\widetilde{R}_{N,k}$ have nonzero entries in at most $4(k + 1)$ rows.

Notice that a similar argument can be used in the two-dimensional setting if the k subdomains where D identically vanishes have smooth enough boundaries: unfortunately in that case, if N^2 is the global size of the involved Jacobian, then the rank correction will grow as N with constant proportional to K and therefore the quality of the corresponding clusters will be lower.

Now, due to the corresponding direct-sum structure of the Jacobian and of the preconditioner and owing to the constant rank of $R_{N,k}$ and $\tilde{R}_{N,k}$, we have clustering at one of $\{(X_N^{(1)}(\mathbf{u}))^{-1}F'(\mathbf{u})\}$ if we have the same clustering for $\{(X_N^{(1)}(\mathbf{u})|_{K_j})^{-1}F'(\mathbf{u})|_{K_j}\}$, for every $j = 0, \ldots, k + 1$. In other words, the statement of the clustering in this setting reduces completely to Theorem 4.14.

We end this section observing that the two-dimensional case can be treated in a similar fashion but with weaker results. Since in this case, due to the non-linearity, it is not possible to symmetrize X_N by a similarity transformation, we limit ourselves to determine the singular value distribution. To this end, it suffices to replace S_N in (4.2) with $S_N^{(2)} = \frac{1}{h} I_{N^2}$ Following the proof of Theorem 4.14 in a two-dimensional setting and using Theorem 3.8 in [15] it holds

$$\{(X_N^{(2)}(\mathbf{u}))^{-1} F'(\mathbf{u})\} \sim_\sigma (1, G), \tag{4.11}$$

where $G = [0,1]^2 \times (0, 2\pi)^2$. Unfortunately, in the two-dimensional case a similarity transform like equation (4.10) does not hold even assuming $\frac{\partial D(u(x))}{\partial u} \geq 0$ and so the existence an eigenvalue cluster can not be easily proved.

The difficulty in the solution of a linear system with coefficient matrix $F'(\mathbf{u})$ is now moved to the solution of a linear system with coefficient matrix $X_N^{(d)}(\mathbf{u})$. From Proposition 4.13 we have that $X_N^{(d)}(\mathbf{u})$ is a M-matrix and the algebraic multigrid (AMG) is well-known to be an optimal solver for M-matrices. A detailed description of the AMG can be found in [12] or [18].

Remark 4.16. The AMG described in [12] converges with a convergence factor independent of the size of the problem when applied to a linear system with a symmetric M-matrix (see Theorem 5.5 in [12]). Therefore the AMG is an effective solver for $X_N^{(d)}(\mathbf{u})$ since it is a M-matrix and it can be rescaled to be symmetric. If we combine the latter statement with the fact that $X_N^{(d)}(\mathbf{u})$ ensures clustering at 1 when used as preconditioner for $F'(\mathbf{u})$, then we can conclude that we have an effective AMG-preconditioning solver for the whole system with coefficient matrix $F'(\mathbf{u})$. Indeed the numerical experiments in the last section will clearly show that the proposed strategies work optimally (or quasi optimally when the grid function is highly nonlinear) with a total computational cost which is linear (or almost linear) with respect to the size N of the involved matrices.

5. Marble sulfation

In [13] simulations for the sulfation of marble on the surface of monuments are described. This phenomenon is the transformation of $CaCO_3$ of the marble stone into $CaSO_4 \cdot 2H_2O$ (gypsum), that is triggered in a moist atmosphere by the availability of SO_2 at the marble surface and inside the pores of the stone.

The mathematical model employed in [13] was described in [1]. The two main variables of the model are $c(t, x)$ denoting the local concentration of calcium carbonate and $s(t, x)$ for the local concentration of SO_2. As the reaction proceeds, the calcium carbonate concentration is reduced from the initial value c_0, as $CaCO_3$ is progressively replaced by gypsum. The porosity of the marble-gypsum mixture is assumed to be the linear interpolation between the porosities of pure-marble and pure-gypsum phases, namely $\varphi(c) = \alpha c + \beta$ for constants α and β such that $\varphi(c) > 0$ for $c > 0$. The model considered is thus described by the following system of PDEs:

$$\begin{cases} \dfrac{\partial \varphi(c)s}{\partial t} &= -\frac{a}{m_c}\varphi(c)sc + d\nabla \cdot (\varphi(c)\nabla s), \\ \dfrac{\partial c}{\partial t} &= -\frac{a}{m_s}\varphi(c)sc. \end{cases} \tag{5.1}$$

The parameters m_s and m_c are fixed by the physical properties of the species involved in the reaction and make sure that the mass balance is fulfilled. On the other hand a represents the reaction

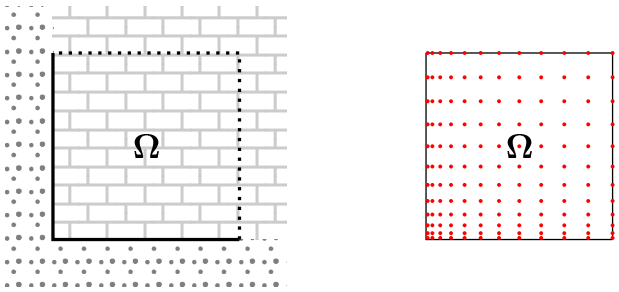

Figure 1: Sample two-dimensional domain Ω for problem (5.1). In the left panel, the "brick pattern" area represents the marble stone, while the dotted area is air. The boundary is drawn with a solid line where Dirichlet boundary conditions are applied and with a dotted line where free-flow boundary conditions are imposed. In the right panel we show the $x_{i,j}$ points of a non-uniform grid.

rate and it depends (among other things) on the moisture of the air and on the temperature, but we keep it constant in this work.

The spatial domain Ω where (5.1) is set represents a piece of marble stone, for which at least a portion of the boundary $\partial\Omega$ is in contact with the polluted atmosphere. In particular $\partial\Omega$ is, in general, split into two parts: one represents the outer surface of the marble sample, in contact with the air, and the complementary part that separates the portion of the marble object of the simulation and the rest of the monument (see Figure 1). Boundary conditions are set, by imposing the value of s on the outer boundary and by imposing free-flow conditions for s on the inner boundary. Since a boundary layer separating the outer gypsum crust from the inner pristine marble emerges at the Dirichlet boundaries, we employ nonuniform grids as depicted in Figure 1 in order to better resolve the solution there.

The general setup for the scheme is the same as in the scalar case: first discretize the time variable using (1.2) and then discretize the spatial domain and the elliptic differential operator with finite differences, write the time-advancement problem as an implicit equation and set up a Newton scheme for solving it.

5.1. One space dimension

We consider $\Omega = [0, 1]$ and the grid points $x_k = g(k/N)$ for a nondecreasing differentiable function $g : [0, 1] \to [0, 1]$ such that $g(0) = 0$ and $g(1) = 1$. For $g(t) = t$ we would obtain the uniform grid employed in [13].

In this problem, the reaction rate a can be considered as a singular perturbation parameter and, for $a \to \infty$, the solution tends to the solution of a Stefan problem [8]. Moreover, for finite a and for the boundary conditions of interest, the functions $c(t, x)$ and $s(t, x)$ are nondecreasing (respectively non-increasing) for $x > 0$ and present a sharp transition from the boundary value 0 (respectively s_0) to c_0 (respectively 0). As noted in [1], the change of variables $x = a\xi$ and $t = a^2\tau$ completely removes the parameter a from the system. Thus the sup-norm of the x-derivative of the solution should scale as $O(a)$. This suggests the use of a Bakhvalov mesh generated by the function

$$g(t) = \begin{cases} \chi(t) = -\frac{\sigma}{a} \ln\left(\frac{q-t}{q}\right) & \text{for } t \in [0, \tau] \\ \pi(t) = \chi(\tau) + \chi'(\tau)(t - \tau) & \text{for } t \in (\tau, 1] \end{cases} \tag{5.2}$$

The parameter q controls how many points are taken in the nonuniform portion of the mesh (we set $q = 0.5$), while σ controls the grading of the mesh, that is how much can vary the size of two neighbouring intervals. In order to accommodate for the movement of the boundary layer towards the interior of the domain, we take a very large value of $\sigma \sim \sqrt{a}$, that sets up a fine nonuniform mesh on a thick enough area. It is worth pointing out that the choice of mesh will affect the convergence of the approximation of the solution of the PDE, but, to a large extent, not the convergence of the methods for the nonlinear system and the preconditioner for the Jacobian that are studied here below.

We denote the midpoints by $x_{k+1/2} = (x_{k+1} + x_k)/2$ and employ two staggered grids in the domain Ω: the set of points x_j ($j \in \mathbb{N}$) carrying the unknowns s_j^n for $s(t^n, x_j)$ and the set of points $x_{j+1/2}$ ($j \in \mathbb{N}$) with the unknowns $c_{j+1/2}^n$ for $c(t^n, x_{j+1/2})$. The shorthand notation $\varphi_{j+1/2}^n = \varphi(c_{j+1/2}^n)$ will also be used.

We describe explicitly only the equations for a generic node away from the boundary, but the boundary conditions can be easily imposed setting the value of s_0 and considering ghost points on the $x = 1$ boundary.

We approximate the elliptic operator along the same lines as in (2.1) with the second order finite difference formula

$$\partial_x(\varphi(c)\partial_x s)|_{x_j} \simeq \frac{\varphi(c(x_{j+1/2}))\frac{s(x_{j+1})+s(x_j)}{h_{j+1}} - \varphi(c(x_{j-1/2}))\frac{s(x_j)+s(x_{j-1})}{h_j}}{(h_j + h_{j+1})/2} \tag{5.3}$$

and the other terms as

$$\varphi(c)s|_{x_j} = \frac{h_{j+1}\varphi(c_{j-1/2}) + h_j\varphi(c_{j+1/2})}{h_j + h_{j+1}} s_j, \tag{5.4a}$$

$$\varphi(c)sc|_{x_j} = \frac{h_{j+1}\varphi(c_{j-1/2})c_{j-1/2} + h_j\varphi(c_{j+1/2})c_{j+1/2}}{h_j + h_{j+1}} s_j, \tag{5.4b}$$

$$\varphi(c)s|_{x_{j-1/2}} = \varphi(c_{j-1/2})\frac{s_j + s_{j+1}}{2} c_{j-1/2}. \tag{5.4c}$$

Note the two different kinds of averaging procedures required in the first, second and last lines: $x_{j+1/2}$ is the midpoint between x_j and x_{j+1}, but x_j is not the midpoint between $x_{j+1/2}$ and $x_{j-1/2}$.

Thus the tridiagonal matrix representing the elliptic operator in (5.1) is $-L_\varphi = -L^{(1)}_{\varphi(\mathbf{c}^n)}$ and is defined as in (2.2). Introducing the $N \times N$ matrices

$$\Phi(\mathbf{c}) = \mathrm{diag}_k^N \left[\frac{h_k\varphi(c_{k+1/2}) + h_{k+1}\varphi(c_{k-1/2})}{h_k + h_{k+1}} \right], \tag{5.5a}$$

$$C(\mathbf{c}) = \mathrm{diag}_k^N \left[\frac{h_k\varphi(c_{k+1/2})c_{k+1/2} + h_{k+1}\varphi(c_{k-1/2})c_{k-1/2}}{h_k + h_{k+1}} \right], \tag{5.5b}$$

$$S(\mathbf{c}, \mathbf{s}) = \mathrm{diag}_k^N \left[\varphi(c_{k+1/2}) \left(\frac{s_{k+1} + s_k}{2} \right) \right], \tag{5.5c}$$

our scheme computes s_j^n and $c_{j+1/2}^n$ with the θ-method for time differencing, namely as the solu-

tion of the following system of equations

$$\begin{cases} 0 = \mathbf{F}^{(s)}(\mathbf{s},\mathbf{c}) = \ \Phi(\mathbf{c})\mathbf{s} - \Phi(\mathbf{c}^{n-1})\mathbf{s}^{n-1} + \theta\Delta t\dfrac{a}{m_c}C(\mathbf{c})\mathbf{s} + \theta\Delta t dL^{(1)}_{\varphi(\mathbf{c})}\mathbf{s} \\ \qquad\qquad + \theta\Delta t\mathbf{b}(\mathbf{c}) + (1-\theta)\Delta t\dfrac{a}{m_c}C(\mathbf{c}^{n-1})\mathbf{s}^{n-1} \\ \qquad\qquad + (1-\theta)\Delta t dL^{(1)}_{\varphi(\mathbf{c}^{n-1})}\mathbf{s}^{n-1} + (1-\theta)\Delta t\mathbf{b}(\mathbf{c}^{n-1}), \\ 0 = \mathbf{F}^{(c)}(\mathbf{s},\mathbf{c}) = \mathbf{c} - \mathbf{c}^{n-1} + \theta\Delta t\frac{a}{m_s}S(\mathbf{c},\mathbf{s})\mathbf{c} + (1-\theta)\Delta t\frac{a}{m_s}S(\mathbf{c}^{n-1},\mathbf{s}^{n-1})\mathbf{c}^{n-1}. \end{cases} \tag{5.6}$$

Equations (5.6) are not linear, since also the matrices C, S, L_φ and Φ depend on $\mathbf{c}^n$ and $\mathbf{s}^n$, either directly or via the function φ. Obviously, for $g(t) = t$, formulae above reduce to those of [13]. The terms involving the function $\mathbf{b}$ are the Neumann boundary terms and will be disregarded in the theoretical considerations below.

Both Crank-Nicholson ($\theta = \frac{1}{2}$) and Implicit Euler ($\theta = 1$) give rise to an unconditionally stable scheme and we employ Newton iterations to solve the nonlinear problem (5.6). To this end, one needs the Jacobian matrix, which is naturally split into four $N \times N$ block as

$$J = F' = \left[\begin{array}{c|c} J^s_s & J^s_c \\ \hline J^c_s & J^c_c \end{array}\right], \qquad\qquad \mathbf{u} = \begin{pmatrix}\mathbf{u}_s \\ \mathbf{u}_c\end{pmatrix}. \tag{5.7}$$

We now describe in more detail its entries, disregarding fixed rank corrections for the boundary conditions. In particular,

$$J^s_s = \Phi(\mathbf{c}) + \theta\Delta t\frac{a}{m_c}C(\mathbf{c}) + \theta\Delta t\, d\, L^{(1)}_{\varphi(\mathbf{c})}, \tag{5.8}$$

$$J^c_c = \mathsf{diag}^N_k\left[1 - \theta\Delta t\frac{A}{m_s}\frac{s_{k-1}+s_k}{2}\left(\varphi'(c_{k-1/2})c_{k-1/2} + \varphi(c_{k-1/2})\right)\right], \tag{5.9}$$

$$J^c_s = \theta\Delta t\,\mathsf{tridiag}^N_k\left[\tfrac{1}{2},\tfrac{1}{2},0\right]\mathsf{diag}^N_k\left[\varphi(c_{k-1/2})c_{k-1/2}\right], \tag{5.10}$$

$$J^s_c = \widetilde{\Phi}(\mathbf{c},\mathbf{s}) + \theta\Delta t\frac{A}{m_c}\widetilde{C}(\mathbf{c},\mathbf{s}) - \theta\Delta t\, d\, Y^{(1)}_N(\mathbf{s}), \tag{5.11}$$

where $Y^{(1)}_N(\mathbf{s})$ is computed as in (3.3c), but using $\mathbf{s}$ in place of $\mathbf{u}$ and $\varphi'(\mathbf{c})$ in place of $D'(\mathbf{u})$ and

$$\begin{aligned} \widetilde{\Phi}(\mathbf{c},\mathbf{s}) &= \mathsf{tridiag}^N_k\left[0, \tfrac{h_{k+1}}{h_k+h_{k+1}}s_k\varphi'(c_{k-1/2}), \tfrac{h_k}{h_k+h_{k+1}}s_k\varphi'(c_{k+1/2})\right], \\ \widetilde{C}(\mathbf{c},\mathbf{s}) &= \mathsf{tridiag}^N_k\left[0, \tfrac{h_{k+1}}{h_k+h_{k+1}}s_k(\varphi'(c_{k-1/2})c_{k-1/2} + \varphi(c_{k-1/2})),\right. \\ &\qquad \left.\tfrac{h_k}{h_k+h_{k+1}}s_k(\varphi'(c_{k+1/2})c_{k+1/2} + \varphi(c_{k+1/2}))\right]. \end{aligned}$$

5.2. Two space dimensions

In two space dimensions we consider the grid points $x_{i,j} = (g^{[1]}(i/N), g^{[2]}(j/N))$ and the staggered grid of the points $x_{i-1/2,j-1/2}$ with abscissae $\frac{1}{2}(g^{[1]}((i-1)/N) + g^{[1]}(i/N))$ and ordinates $\frac{1}{2}(g^{[2]}((j-1)/N) + g^{[2]}(j/N)))$. The unknowns s_{ij} for $i, j = 1,\dots,N$ are collected in lexicographic order into the vector $\mathbf{s}$, while the unknowns $c_{i-1/2,j-1/2}$ for $i, j = 1,\dots,N$, are collected in lexicographic order into the vector $\mathbf{c}$. (See Figure 1 for an example)

Each time step requires the solution of a nonlinear equation in $2N^2$ unknowns that can still be represented by formula (5.6), with the matrices described here below. The differential operator

is represented by a matrix (denoted $L^{(2)}_{\varphi(\mathbf{c})}$) that has the sparsity pattern of the tensor product $L^{(1)}_{\varphi(\mathbf{c})} \otimes I + I \otimes L^{(1)}_{\varphi(\mathbf{c})}$ and with entries computed as those of $L^{(2)}_D$ (see Section 2.2).

The other matrices appearing in (5.6) are the two-dimensional analogues of the (5.5). For example, matrices Φ and C are again diagonal and have entries obtained with weighted averaging in both the x and the y directions since we approximate

$$c_{ij} \simeq \frac{h_i}{h_i + h_{i+1}} \left(\frac{h_j c_{i+1/2,j+1/2} + h_{j+1} c_{i+1/2,j-1/2}}{h_j + h_{j+1}} \right) + \frac{h_{i+1}}{h_i + h_{i+1}} \left(\frac{h_j c_{i-1/2,j+1/2} + h_{j+1} c_{i-1/2,j-1/2}}{h_j + h_{j+1}} \right)$$

in perfect analogy with formulae (5.4a) and (5.4b). Averaging the s variables in (5.4c) can again be performed with fixed weights also on nonuniform grids. The main difference with the one-dimensional case is that each entry of $\Phi^{(2)}$ and $C^{(2)}$ depend on four unknowns in $\mathbf{c}$ (e.g. $c_{i\pm1/2,j\pm1/2}$) and each entry of S now depends on four unknowns in $\mathbf{s}$ (e.g. $s_{i+\varepsilon,j+\varepsilon}$ for $\varepsilon = 0, 1$).

Correspondingly, the Jacobian has the same 2×2 block structure as in the one-dimensional case, but now

$$J^s_s = \Phi^{(2)}(\mathbf{c}) + \theta \Delta t \frac{a}{m_c} C^{(2)}(\mathbf{c}) + \theta \Delta t L^{(2)}_{\varphi(\mathbf{c})}$$

which is a diagonal correction of order $O(1 + \Delta t)$ to the penta-diagonal matrix representing the elliptic operator. Moreover the J^s_c and J^c_s blocks have now nonzero entries on four diagonals, while the J^c_c block is again diagonal.

5.3. Solving the linear system

At each Newton iteration, one has to solve a linear system with matrix J, which is not symmetric and thus GMRES is a natural choice for the main Krylov solver. In order to devise a preconditioning strategy, we follow the proposal in [13]. We observe that the lower left block J^c_s has nonzero entries only on two diagonals (respectively four, in two space dimensions) and these decay as $O(\Delta t)$, while the bottom right block J^c_c is the identity matrix plus a diagonal matrix with $O(\Delta t)$ entries.

Theorem 5.1 ([13])**.** *Assuming $\Delta t = h = \frac{1}{N+1}$, the upper triangular part of J in* (5.7)*, namely*

$$P = \left[\begin{array}{c|c} J^s_s & J^s_c \\ \hline \mathbf{0} & J^c_c \end{array} \right], \tag{5.12}$$

is an optimal preconditioner for J, both in one and two space dimensions, assuming that the function $\varphi(c)$ in (5.1) *is bounded away from* 0 *(i.e. when the porosity of the gypsum-carbonate mixture is never zero).*

Remark 5.2. When applying the preconditioner P in (5.12), the block triangular system $P\mathbf{y} = \mathbf{b}$ is solved as

$$\mathbf{y}_c = (J^c_c)^{-1} \mathbf{b}_c$$

and

$$\mathbf{y}_s = (J^s_s)^{-1} (\mathbf{b}_s - J^s_c \mathbf{y}_c), \tag{5.13}$$

where the the sub/super-script s and c stand for the upper half and to the lower half of the vectors, respectively. Theorem 5.1 shows that the spectrum of $P^{-1}J$ is strongly clustered at 1

independently on the discretization parameter h and thus the block-preconditioner P is optimal. The matrix J_c^c is easily inverted since it is a diagonal matrix. On the other hand, the matrix J_s^s can not be easily inverted, especially for multidimensional problems and small values of β. Therefore, an optimal solver for the J_s^s block is needed for obtaining an efficient global method.

We point out that there are many similarities between the J_s^s block and the Jacobian matrix (3.3a). In fact, with respect to (3.3a), the identity is replaced by a diagonal matrix with $O(1)$ entries $(\Phi + \theta\Delta t \frac{a}{m_c} C)$, while the tridiagonal $Y_N^d(\mathbf{u})$ term is not present in J_s^s, corresponding instead to the third term of the J_c^s block. Hence J_s^s is spectrally not too different from $X_N(\mathbf{u})$ in (3.3a). Thus we expect that the unpreconditioned GMRES applied to the linear system (5.13) has an iterations count that grows similarly to the one for $F'(\mathbf{u})$ of (3.3a). In [5] there is a discussion of such growth in the case of uniform grids, while in in Subsection 6.1 we provide some numerical evidence in the case of nonuniform grids.

The previous discussion suggests to use the AMG preconditioner for the coefficient matrix J_s^s, in analogy with the strategy discussed in Subsection 4.2 for the coefficient matrix $F'(\mathbf{u})$. Indeed, when $\beta > 0$ the matrix $L_{\phi(\mathbf{c})}^{(d)}$ is a M-matrix and the diagonal matrix $\Phi + \theta\Delta t \frac{a}{m_c} C$ has positive entries, thus J_s^s is a M-matrix and the AMG is a optimal preconditioner for the linear system (5.13).

In conclusion, we solve the linear system of the Jacobian J in (5.7) using the P-GMRES with the preconditioner P defined in (5.12) and where the linear system (5.13) is solved only approximately by employing just one V-cycle iteration of the AMG algorithm.

6. Numerical tests

Numerical tests were performed in MatLab 7.0, exploiting the MatLab interface to the AMG library of [10]. In particular, the algebraic multigrid preconditioner was the one provided by the function `hsl_mi20_precondition` with the following choices: the smoother is the damped Jacobi method with damping parameter set to $2/3$, `1` pre-smoothing and `1` post-smoothing iteration were used, coarsening is halted if less than `9` points are left in the coarse mesh or if all rows in the coarse matrix do not have a negative off-diagonal element. All other parameters were left to their default values.

In Subsection 6.1, we present tests on the predictions of the theory developed in Section 4, while Subsection 6.2 is devoted to the model described in Section 5. Finally 6.3 is about the convergence of the Newton method.

6.1. Scalar, degenerate, equation

The purpose of the following tests is to highlight the features of the approximation techniques developed in the paper. Therefore, we start with a monodimensional example, even if iterative methods are not necessary since the linear system with diagonally dominant tridiagonal matrices can be efficiently solved by a direct method, because the asymptotic behaviour can be easily estimated showing that the numerical results agree with the theoretical analysis provided in the previous sections. To this end, we consider the scalar equation (1.1) for $D(u) = mu^{m-1}$ for $m > 1$ and approximate numerically the self-similar exact solutions

$$u(t,x) = t^{-\alpha}\left[1 - \alpha\tfrac{m-1}{2m}\left(|x|(t+1)^{-\alpha}\right)^2\right]_+^{\frac{1}{m-1}}, \qquad \alpha = \tfrac{1}{m+1} \tag{6.1}$$

due to Barenblatt and Pattle [19] (the + subscript denotes the positive part). The exact solution features singular points that move towards the boundary of the domain at finite speed (Figure 2a), and it is nonzero and smooth in between these points and zero outside.

Although for this kind of equations one would naturally employ adaptive mesh refinement techniques, we solve the problem on a set of nonuniform fixed meshes, varying the distribution of the mesh points in the domain. The tests confirm the (obvious) remark that employing too many points in the smooth region at the centre of the domain is detrimental for the error of the scheme, but more surprisingly that doing so also puts unwanted extra stress on the solver, since the condition number of the linear systems may grow dramatically. This is accurately predicted by the theory of §4 and verified here below. On the side, we also show that AMG preconditioning remains optimal even with the worst choice of meshes considered here.

In particular we consider the meshes generated by the grid functions $g_\alpha : [-1, 1] \to [-1, 1]$ defined by

$$g_\alpha(t) = \mathtt{sign}(t)|t|^\alpha$$

Note that g_1 corresponds to the uniform mesh, while choosing $\alpha \neq 1$ generates a weakly regular mesh that is finer in the middle of the domain ($\alpha > 1$) or at the endpoints ($\alpha \in (0, 1)$). We also consider two regular meshes of Shishkin and Bakhvalov type (see [11]). A mesh of each kind (with 32 points) is depicted at the bottom of Figure 2a.

Condition number. First note that a direct consequence of the spectral analysis in Section 4.2 is that introducing a grid refinement at a point where the diffusion coefficient is not degenerate has adverse consequences on the condition number of the Jacobian matrix.

For the one-dimensional case, we consider $A_N^{(1)} = hF'(\mathbf{u})$ since the spectral condition number is not affected from constant scaling. From the proof of Theorem 4.14, see in particular equation (4.5), it follows that $\{A_N^{(1)}\} \sim_\lambda (\psi_A, G)$, where $G = [0, 1] \times (0, \pi)$ and

$$\psi_A(x, s) = \theta w^{[D]}(x)(2 - 2\cos(s)),$$

with

$$w^{[D]}(x) = \begin{cases} \frac{D(u(g(x)))}{g'(x)^2}, & \text{if } g'(x) \text{ is defined and nonzero,} \\ 1, & \text{otherwise,} \end{cases}.$$

Hence, the spectral condition number of $A_N^{(1)}$ can be estimated since the largest eigenvalue grows as the order of strongest pole in $\psi_A(x, s)$, i.e., in $w^{[D]}(x)$. The hI_N term in $A_N^{(1)}$ implies that the smallest eigenvalue goes to zero as $\lambda_{\min} \sim 1/N$. The strongest divergence of $\lambda_{\max}$ may arise from the first term, especially when $g'(x)$ has a zero where the numerator does not vanish: in this situation, the largest eigenvalue of $A_N^{(1)}$ would grow as $\lambda_{\max} \sim N^{2q}$ if $g'(x)$ has a zero of order q. The resulting spectral condition number then grows as N^{2q+1}. This actually happens in our tests when using the g_2- and g_3-generated grids, since in these cases the zero of g' is at $x = 0$, where the solution u of (6.1) is nonzero.

In particular we computed solutions for the one-dimensional Barenblatt problem with $m = 3$, final time $20/32$, $\Delta t = 1/N$ and N ranging from 32 to 4096. During the computations we estimated the spectral condition number of the Jacobian matrix (`condest` in MatLab) and, in different runs, the number of iterations used by GMRES without preconditioner, with Jacobi preconditioner and with the AMG V-cycle preconditioner were recorded. Table 1 collects all data, as well as the CPU time used for the setup of preconditioners and linear system solves during a complete simulation on the $N = 4096$ grids.

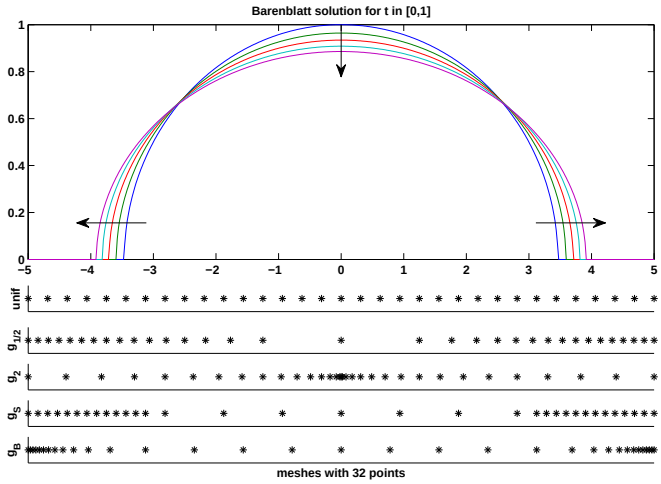

(a)

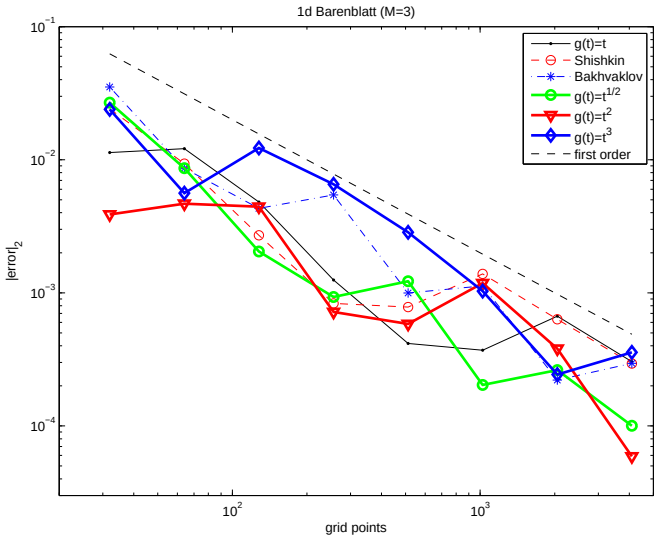

(b)

Figure 2: Exact Barenblatt solution (arrows indicate the direction of time evolution) and meshes with 32 points (a) and Euclidean norm of the error at the final time for the Barenblatt equation (6.1) in one space dimensions (b). Thin lines are regular meshes, thick ones are weakly regular meshes.

1D mesh	cond(J)	GMRES iterations			Newton iterations	GMRES CPU time		
		no P	Jac	AMG		no P	Jac	AMG
unif	$N^{0.97}$	$N^{0.42}$	$N^{0.47}$	2.54	2.24	1058	1892	45
Shish	$N^{1.14}$	$N^{0.46}$	$N^{0.48}$	2.73	3.00	1466	2590	93
Bakh	$N^{0.85}$	$N^{0.29}$	$N^{0.41}$	2.37	2.00	925	1821	55
$g_{1/2}$	$N^{0.94}$	$N^{0.38}$	$N^{0.44}$	2.50	2.99	1343	2194	85
g_2	$N^{3.00}$	$N^{0.76}$	$N^{0.70}$	3.47	2.01	17558	41721	86
g_3	$N^{5.00}$	$N^{0.83}$	$N^{0.78}$	3.83	2.02	n/a	159993	88

Table 1: Regular (at the top) and weakly regular (bottom) grid functions for $\theta \in [-1, 1]$. Condition number of the Jacobian matrix, average number of GMRES iterations per Newton step, average number of Newton iterations per timestep, for N ranging from 32 to 4096. The last columns are the CPU times in seconds spent on GMRES (including setup of preconditioners) for a complete run on the largest grid. (The unavailable data is due to GMRES stagnation). The sub-columns refer to the preconditioning strategy used inside GMRES (unpreconditioned, Jacobi, AMG V-cycle).

These data confirm the prediction on the growth of the condition number and also the optimality of our preconditioning strategy: in all cases considered, the number of GMRES iterations grows with N, but the PGMRES iterations (where the preconditioner is one AMG V-cycle) remains constant with respect to N and suffers only a very moderate increase with the worsening of the grid irregularity.

For g_α with $\alpha = 4, 5$, we observe a growth of the condition number with the number of grid points with the laws N^7 and N^9, respectively. We did not report the result in the table since the Newton method has difficulties to converge in these extreme cases. In such cases the use of other nonlinear solvers with guaranteed convergence should be considered at the beginning (see e.g. [3]). Also, we do not report data for the two-dimensional cases, since they show a similar pattern as the one-dimensional ones discussed here.

Errors. In Figure 2b we compare the errors at the final time recorded in the previous runs. We consider the Crank-Nicholson time integration scheme with various choices for the spatial mesh. We observed that this method leads to lower errors than the Implicit Euler method, but its theoretical order of convergence is not reached owing to the non-regularity of the solution, which has a compact support expanding in time, with two non differentiable points with vertical tangent at the boundary of the support.

Also in terms of the error reduction, we see that the meshes with most points in the middle of the domain perform most poorly (see g_2 and g_3), while uniform meshes or meshes with additional points where the discontinuity in u_x travels give rise to more regular convergence histories. Among these, the error reduction is more regular for meshes generated with smoother generating function, as shown by the series $g_{1/2}$, g_B, g_S.

The same comments extend to the results for the two-dimensional simulations.

6.2. Sulfation model

For the marble sulfation problem, we consider a situation that models the deterioration at an edge of a monument. We report the solution of the model at the final time of the simulation, as well as studies of the performance of the preconditioners and various measures of the error committed at different grid sizes, comparing uniform and non-uniform meshes. We fix, as in [1], the physically correct values $d = 0.1$, $m_s = 64.06$, $m_c = 100.09$, $\alpha = 0.01$, $\beta = 0.1$, and integrate the equations in time up to $t_{fin} = 1$. As explained in [1], a controls the reaction rate and thus the temporal scale of the PDE; in particular it depends on other ambient parameters (mainly

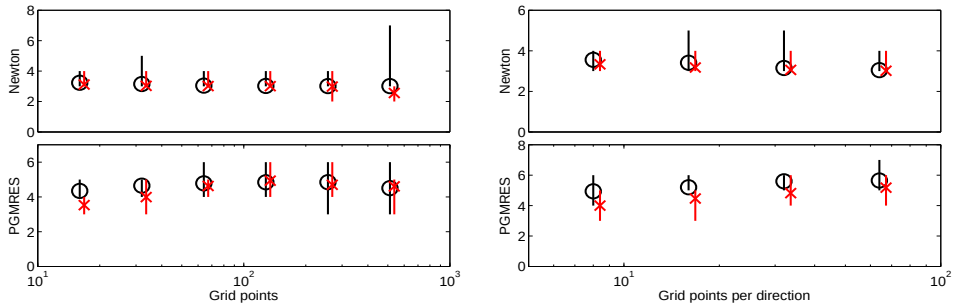

(a) (b)

Figure 3: Newton iterations and PGMRES iterations recorded during marble sulfation simulations in one (a) and two (b) space dimensions. Symbols indicate the median and the whiskers extend from the minimum to the maximum value. Red crosses refer to the uniform grids and black circles to the Bakhvalov grids. In these tests the Crank-Nicholson scheme was used.

temperature and humidity) and it is a lot harder to measure: here we fix it to the reasonable value $a = 10^4$ as in [1].

This model prescribes boundary conditions of Dirichlet type at $x = 0$ (and also at $y = 0$ in the two-dimensional case), that are not consistent with the initial data: in fact the simulations start with no SO_2 inside the marble and impose a nonzero SO_2 concentration in the surrounding air. This inconsistency gives rise to oscillations due to fact that Crank-Nicholson ($\theta = \frac{1}{2}$) is not L_0-stable. Here we take the simple approach to replace the first Crank-Nicholson step with two Implicit Euler ($\theta = 1$) steps with $\Delta t = 1/2N$. (Note that another approach would be to use the three stages diagonally implicit L_0-stable Runge-Kutta of second order described in [4].)

Preconditioning. In Figure 3 we show the number of Newton iterations needed to perform a simulation with model (5.1) in one and two-dimensional square domains varying the number of grid points N, with uniform and Bakhvalov grids. We point out that the number of iterations is very small and tends to become lower with increasing N, due to the fact that the grid resolves better the boundary layer. The lower portions of the graphs show the number of preconditioned GMRES iterations needed for the linear solves. This is almost constant across the whole range of values of N, showing the optimality of the preconditioning strategy. Moreover the number of PGMRES iterations never exceeds 6, so that there is no need to employ restarting strategies in the GMRES algorithm. We note that thanks to the AMG preconditioner, the use of a non-uniform grid does not increase the computational cost with respect to employing a uniform grid, while the quality of the solution improves a lot, in particular close to the boundary layers.

Result of the simulations. Figure 4 shows the contour plot of the solution obtained at time $t = 1$ with the Crank-Nicholson method, using a Bakhvalov grid of 64×64 points. We observe that the carbonate-gypsum boundary layer has a more rounded and plausible shape that the one obtained in [13]. This is due to the improvement of resolution granted by the non-uniform grid.

The plot in Figure 5 shows the profiles of calcium carbonate (c variable) and SO_2 content (s variable) along the diagonal of the domain (the bisector of the first quadrant), the x-axis being labelled with the distance from the corner. The picture clearly shows the higher resolution power of the non-uniform grid: when using uniform grids, one needs 64 points to obtain the same

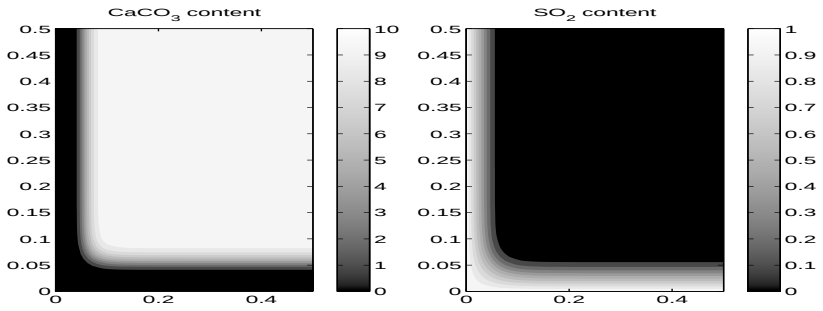

Figure 4: Contour plot of the solution obtained at time $t = 1$ with the Crank-Nicholson method, using a Bakhvalov grid of 64×64 points.

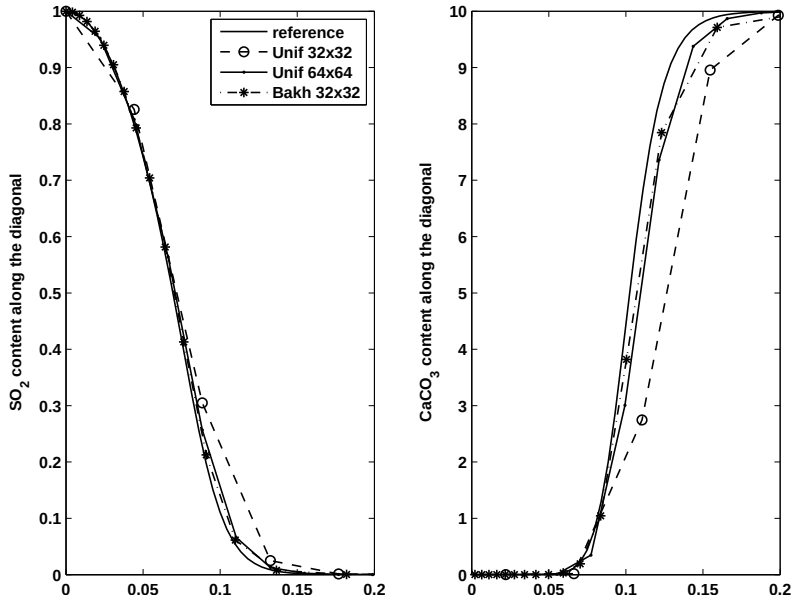

Figure 5: Profile of the solutions along the diagonal $x = y$ at $t = 1.0$ obtained with the Crank-Nicholson and Implicit Euler schemes, uniform and Bakhvalov grids.

	$\|E_c\|_\infty$	rate	$\|E_c\|_1$	rate	$\|E_c\|_2$	rate		$\|E_f\|_2$	rate
U16 × 16	7.27		1.69		6.58E-2			0.91	
U32 × 32	3.97	0.87	0.60	1.48	2.92E-2	1.17		0.34	1.41
U64 × 64	1.29	1.61	0.18	1.68	9.55E-3	1.61		0.14	1.26
G16 × 16	3.54		0.85		3.57E-2			0.32	
G32 × 32	1.39	1.34	0.25	1.79	1.21E-2	1.56		0.16	1.02
G64 × 64	0.42	1.72	0.06	2.09	2.91E-3	2.05		0.10	0.68
B16 × 16	3.23		0.73		2.94E-2			0.26	
B32 × 32	0.72	2.15	0.14	2.33	6.46E-3	2.18		0.14	0.89
B64 × 64	0.16	2.13	0.03	2.46	1.21E-3	2.42		0.11	0.36

Table 2: Errors in various norms for the $CaCO_3$ profile along the diagonal of the computational domain for uniform (U), Gauss-Lobatto (G) and Bakhvalov (B) meshes of different dimensions. E_c denotes the error at final time on the c variable and E_f (last two columns) denotes the error in the function describing the front position versus time.

resolution of the boundary layer achieved the 32 points Bakhvalov grid. This is accomplished also thanks to a more accurate and steeper profile of the s variable whose values are less affected by numerical diffusion. The data shown were obtained with the Crank-Nicholson scheme. We observed only a small difference in resolution between the two time integration schemes, with Crank-Nicholson being slightly sharper than Implicit Euler. Since the computational cost of the two schemes is almost identical, we favour the Crank-Nicholson one, but this latter observation indicates that in this problem the employment of the second order L-stable scheme of [4] is not cost-effective since it involves the computation of two implicit stages per time step.

Table 2 collects data on the convergence of the algorithm. To this end, errors in the c and s variables were computed by comparing the numerical results with a solution computed on a very fine mesh (indicated by *reference* in the legend of Figure 5). They are listed (in three different norms) together with the convergence rates for meshes of uniform, Gauss-Lobatto (see the Introduction) and Bakhvalov type (see (5.2)). We report the data on the c variable, the other ones being completely analogous. The benefits of nonuniform meshes are apparent from the table, where it can be seen that a generic nonuniform mesh can improve the errors, but that Bakhvalov meshes yield also the optimal (second order) convergence rates. The last column of Table 2 is about the position of the marble-gypsum interface with respect to time, that is important for decision making in real world applications. Such function was estimated from the simulations by looking for the steepest gradient in the profile of c along the diagonal. In this respect, the nonuniform meshes can approximate the front position at a given accuracy by using far less points in the grid.

6.3. Convergence of the Newton method

Finally, Figure 6 shows the graphs of the convergence to zero of the Newton residual in the nonlinear scheme. The left panel is for the Barenblatt problem with $m = 2$ and the right one for the sulfation problem. Curves for the one-dimensional cases refer to 128 grid points while the two-dimensional tests were performed with 32×32 grid points. Data were recorded during the first timestep, with $\Delta t = 1/N$, and the initial guess was the initial data. Performance of the method in later steps or with more grid points is similar and often better, due to a smoother solution or enhanced grid resolutions.

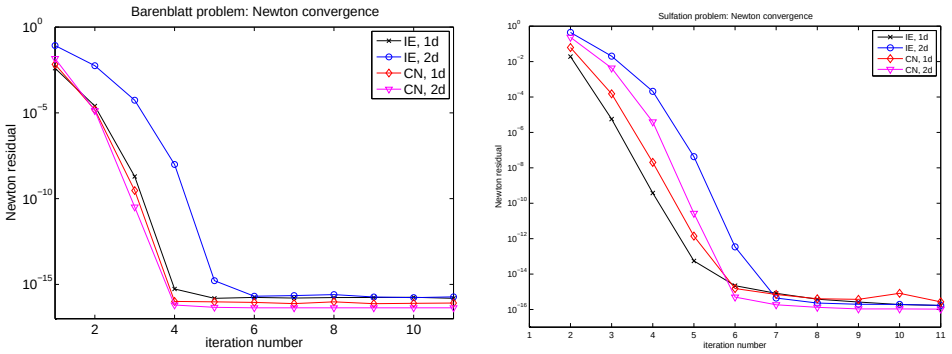

(a) (b)

Figure 6: Decay of Newton residual during the first timestep.

Acknowledgments. The authors wish to thank the anonymous referees for the useful suggestions and comments. This work was partly supported by MIUR (PRIN 2008 N. 20083KLJEZ)

References

[1] D. Aregba Driollet, F. Diele, R. Natalini, A mathematical model for the SO_2 aggression to calcium carbonate stones: numerical approximation and asymptotic analysis., SIAM J. Appl. Math. 64 (2004) 1636–1667.

[2] B. Beckermann, S. Serra-Capizzano, On the asymptotic spectrum of finite element matrix sequences, SIAM J. Numer. Anal. 45 (2007) 746–769.

[3] S. Bellavia, B. Morini, A globally convergent newton-gmres subspace method for systems of nonlinear equations, SIAM J. Sci. Comput. 23 (2001) 940–960.

[4] J. Cash, Two new finite difference schemes for parabolic equations, SIAM J. Numer. Anal. 21 (1984) 433–446.

[5] M. Donatelli, M. Semplice, S. Serra-Capizzano, Analysis of multigrid preconditioning for implicit PDE solvers for degenerate parabolic equations, SIAM J. Matrix Anal. (2011). In press.

[6] L. Golinskii, S. Serra-Capizzano, The asymptotic properties of the spectrum of nonsymmetrically perturbed Jacobi matrix sequences, J. Approx. Theory 144 (2007) 84–102.

[7] U. Grenander, G. Szegő, Toeplitz forms and their applications, Chelsea Publishing Co., New York, 2nd edition, 1984.

[8] F.R. Guarguaglini, R. Natalini, Fast reaction limit and large time behavior of solutions to a nonlinear model of sulphation phenomena, Comm. Partial Differential Equations 32 (2007) 163–189.

[9] R. Horn, C. Johnson, Topics in matrix analysis, Cambridge University Press, Cambridge, 1991.

[10] HSL, A Collection of Fortran codes for large-scale scientific computation., 2007. Available at http://www.hsl.rl.ac.uk.

[11] T. Linß, Layer-adapted meshes for reaction-convection-diffusion problems, number 1985 in Lecture notes in mathematics, Springer, 2010.

[12] J. Ruge, K. Stüben, Algebraic multigrid, in: Multigrid methods, volume 3 of *Frontiers Appl. Math.*, SIAM, Philadelphia, PA, 1987, pp. 73–130.

[13] M. Semplice, Preconditioned implicit solvers for nonlinear PDEs in monument conservation, SIAM J. Sci. Comput. 32 (2010) 3071–3091.

[14] S. Serra-Capizzano, The GLT class as a generalized Fourier analysis and applications, Linear Algebra Appl. 419 (2006) 180–233.

[15] S. Serra Capizzano, C. Tablino Possio, Analysis of preconditioning strategies for collocation linear systems, Linear Algebra Appl. 369 (2003) 41–75.

[16] J. Stoer, R. Bulirsch, Introduction to numerical analysis, volume 12 of *Texts in Applied Mathematics*, Springer-Verlag, New York, third edition, 2002.

[17] P. Tilli, Locally Toeplitz sequences: spectral properties and applications, Linear Algebra Appl. 278 (1998) 91–120.

[18] U. Trottenberg, C.W. Oosterlee, A. Schüller, Multigrid, Academic Press Inc., San Diego, CA, 2001. With contributions by A. Brandt, P. Oswald and K. Stüben.
[19] J.L. Vázquez, The porous medium equation, Oxford Mathematical Monographs, The Clarendon Press Oxford University Press, Oxford, 2007.